

Objective, high-throughput regularity quantification of laser-induced periodic surface structures (LIPSS)[☆]

Eric Rahner^{a,*}, Tobias Thiele^a, Heike Voss^b, Frank A. Müller^a, Jörn Bonse^b, Stephan Gräf^a

^a Friedrich Schiller University Jena, Otto Schott Institute of Materials Research (OSIM), Löbdergraben 32, 07743 Jena, Germany

^b Bundesanstalt für Materialforschung und -prüfung (BAM), Unter den Eichen 87, 12205 Berlin, Germany



ARTICLE INFO

Keywords:

Laser-induced periodic surface structures (LIPSS)
Image processing
Regularity quantification
Fourier analysis
Structural homogeneity
AISI 316L stainless steel
AlMg5 alloy

ABSTRACT

The growing demand for precise surface functionalization through laser-generated periodic surface structures highlights the necessity for efficient, reproducible, and objective evaluation methods to evaluate their structural regularity. We introduce *Regularity* (v.1.2.7), a freely available, Python-based software with a graphical user interface for the automated, quantitative assessment of the regularity of laser-induced periodic surfaces structures (LIPSS), obtained from optical microscopy, SEM, or AFM. The software integrates image segmentation, one- and two-dimensional Fourier analyses, and gradient-based orientation determination to facilitate a comprehensive regularity analysis of grating-like (quasi-)periodic surface patterns with spatial periods Λ . This is achieved through the proposed regularity tuple R , composed of five key parameters: the normalized spread of the spatial period $R_{\Lambda,2D}$ (from 2D-FT), the normalized variation of the most frequent spatial period R_Λ (from 1D-FT), the Gini coefficient G , the Dispersion of the LIPSS Orientation Angle $\delta\theta$ (DLOA), and the mean phase deviation $\overline{\Delta\phi}$. To demonstrate its applicability, we compare ideal sinusoidal patterns with SEM images obtained from LIPSS on stainless steel (AISI 316L) and aluminum alloy (AlMg5) surfaces, confirming the software's ability to objectively distinguish between varying levels of structural regularity. *Regularity* facilitates high-throughput analysis and data-driven process optimization in surface engineering and laser materials processing.

1. Introduction

Laser-based surface structuring refers to the well-defined modification of the surface topography of a material on different length scales with the objective of creating functional surface properties. These may include structural colors, specific wetting states, cell-growth stimulation or suppression, and wear resistance [1–10]. The versatility and flexibility of surface engineering makes it the subject of intensive research into a wide variety of different types of materials and unlocks novel applications, e.g., in medicine, optics, and biology [1–3,11,12].

Extremely short (ultrashort) laser pulses allow to temporally separate the initial stage of energy deposition to the workpiece via absorption of the optical radiation from the subsequent energy relaxation and material removal processes. Thus, during the laser pulse itself, the deposited laser pulse energy stays confined, which enables highly precise processing of material surfaces with feature sizes down to the nanoscale [13]. Furthermore, the large coherence of the laser radiation

enables the use of optical effects such as scattering and interference to create periodic structures at the irradiated surfaces. This includes, amongst others, the self-ordered formation of so-called *laser-induced periodic surface structures* (LIPSS), as well as the controlled generation of almost arbitrarily complex periodic patterns through *direct laser interference patterning* (DLIP). The regularity of these periodic surface structures, often termed homogeneity, is crucial for certain surface properties. The term describes the systematic and ordered arrangement of structural features. Rossi et al. [14] defined the homogeneity H of a system as “the similarity of its components considering a given attribute”. This attribute could be, e.g., the spatial period of the surface pattern. In the context of LIPSS, regularity refers to the homogeneity of the generated periodic structures in terms of their spatial period Λ , orientation, modulation depth h , length of individual LIPSS ridges, local lateral displacement, etc. The regularity of LIPSS is mainly influenced by the complex interplay between laser and processing parameters, along with intrinsic optical, structural (e.g. defects), and topographical

[☆] This article is part of a special issue entitled: 'ICPEPA-2025' published in Applied Surface Science.

* Corresponding author.

properties of the material [15–18]. In the field of optics, plasmonic field enhancements induced during femtosecond (fs) laser irradiation have been identified as playing a pivotal role in the formation of nanoscale gratings [19]. The initial surface morphology and laser beam characteristics are decisive factors: unidirectional roughness strongly affects the achievable regularity [20], while wavefront curvature [21] and high repetition rate processing [22] have been exploited to enhance structural homogeneity. Material properties are equally important, as grain orientation in combination with angle of incidence and laser beam polarization [23] govern nanostructure morphology on stainless steel [18], while substrate microcrystallinity has been demonstrated to determine LIPSS orientation [24]. Beyond these aspects, functional demonstrations highlight the significance of structural order, as evidenced by highly regular one-dimensional (1D) and two-dimensional (2D) subwavelength gratings on metallic films [25] and large-area self-aligned LIPSS [26]. These findings emphasize the technological relevance of scalable regularity control.

The accurate and objective quantification of the regularity is, therefore, a key element to better understand the highly dynamic LIPSS formation process and to be able to improve the desired functionality of the surface. Reliable quantification of the regularity of laser-generated surface structures is not only of academic interest but also directly linked to the reproducibility of functional surface properties. Existing workflows often rely on manual thresholding and subjective evaluation, which hinders comparability across studies and limits their applicability in high-throughput contexts.

In the simplest case, the two-dimensional Fourier transform (2D-FT) of a microscopic image of the structured surface provides information about the dominant spatial frequencies (spatial periods), the orientation and symmetry of the surface pattern, and the presence of defects or irregularities. For LIPSS, the Fourier spectrum typically exhibits sickle-shaped features [6]. The width of these features in reciprocal space is a measure of the regularity of the spatial periods, while the opening angle $\delta\theta$ of the sickles represents the local curvature and alignment of the structures [27]. It is often referred to as the dispersion of the LIPSS orientation angle (DLOA). Although the method is conceptually simple, the practical evaluation of peak position, width and opening angle of the features is strongly user dependent. A step towards (semi)-automated and objective quantification has been taken with mathematical and software-based algorithms, most of which were originally developed in the context of DLIP microstructures and LIPSS. Gnilitskyi et al. [15] employed the ImageJ plug-in *OrientationJ* [28,29] to determine the orientation spectrum of LIPSS, with $\delta\theta$ obtained from a histogram using a threshold criterion. While more objective than purely manual methods, the procedure remains time-consuming for large datasets, and the accuracy of the procedure is influenced by the size of the analyzed image section (region of interest, ROI). Lechthaler et al. [30] proposed a method to quantify the regularity of DLIP structures using the Gini coefficient G . In this approach, the Lorentz curve – a graphical tool commonly used to analyze financial income distributions – is applied to assess the similarity of system components based on the definition of Rossi et al. [9]. According to this procedure, a system is considered perfectly homogeneous if its Lorentz curve is a straight line, corresponding to $G = 1 - H = 0$, where G represents the degree of inequality within the system [14]. Lechthaler et al. chose in this context the surface periodicity as an attribute, which was then analyzed via Fourier transformation and compared across equally sized image segments to calculate G for the entire image. The authors emphasize that G reflects tendencies rather than absolute values, as it depends on the number and size of the selected image segments [30]. Wang et al. [17] combined 2D-FTs with the calculation of G to assess the regularity of DLIP structures. After converting an SEM image into the spatial frequency domain, they extracted the primary spatial frequency profile and computed the Lorenz curve, using the spatial frequencies as the attribute. For highly regular and homogeneous structures, the distribution is concentrated at a single spatial frequency, resulting in $G = 0$ [31]. However, phase information

inherent to the 2D-FT is not considered in these analyses.

This important aspect was addressed by Takenaka et al. [32], who proposed the *Perpendicular, Period and Phase Scanning* (P^3S) method for pixel-precise analysis of the local spatial period and phase evolution of LIPSS. In this approach, the image is divided into single-pixel wide columns perpendicular to the LIPSS ridge orientation, and then the period Λ and phase φ in each column are determined using 1D-FT. The mean value and standard deviation of Λ were used to quantify the regularity of the spatial period, while phase regularity was assessed based on the phase difference between adjacent image segments ($\Delta\varphi$), i.e., the individual pixel-lines of the image. The mean value of $\Delta\varphi$ then indicates directional changes or bifurcations in the LIPSS pattern [32]. Illustrating the growing need for accessible, automated software frameworks in this field Schell et al. [33,34] recently presented *Surfalyze*, a versatile, scripting-centered Python library designed for the efficient analysis of periodic microstructured surfaces.

In addition to the *ex-situ* microscopy-based evaluation of LIPSS, *in-situ* monitoring of their pulse-by-pulse evolution by optical scatterometry [35–37] or by grazing-incidence X-ray scattering in combination with modelling of scattering/diffraction patterns provide a powerful approach for quantifying the degree of order of LIPSS during their processing [38,39]. Recent time-resolved single-pulse pump-probe scattering experiments employing short-wavelength (XUV and X-ray) free-electron lasers have further enabled direct access to the dynamics of LIPSS formation, combining ultrafast temporal resolution with the required nm-scale spatial sensitivity being suitable also for subwavelength-sized LIPSS [40–42]. Together, these *in-situ* scattering techniques constitute a valuable complement to established *ex-situ* imaging methods, offering insights into the transient evolution and ordering processes that are not accessible from post-mortem surface analysis alone.

Despite the available methods and advances in image processing, surface engineering in general and research on LIPSS in particular still lack fully automated analysis tools that perform a comprehensive evaluation of the regularity of quasi-periodic structured surfaces in a standardized and objective manner. Therefore, in this work, the computer program *Regularity* has been developed as a novel free software with a graphical user interface (GUI) that allows an intuitive and fully automated characterization of periodic surface structures. Suitable sources of microscopic images include high-resolution techniques such as scanning electron microscopy (SEM) and atomic force microscopy (AFM). Optical microscopy can also be employed, provided that its spatial resolution remains sufficient to clearly resolve the specific type of LIPSS under investigation. The software enables the simultaneous evaluation of a large number of images on any standard PC. This feature is becoming increasingly important both in modern computational materials science and in the development of technical laser-based processes, as the increasing use of machine learning and artificial intelligence requires the processing of large amounts of data.

After describing the mathematical principles, the functions and performance of the software are discussed using the example of self-ordered LIPSS. For this purpose, LIPSS patterns generated by fs-laser irradiation are compared with each other, as well as with a synthetically generated sinusoidal topographic test pattern as reference featuring ideal regularity. The software can also be used for other periodic surface structure types such as DLIP patterns.

2. Fundamentals

Robust and accurate quantification of the regularity of periodically structured surfaces requires appropriate processing of microscope images. Fig. 1 summarizes the deterministic, fully automated workflow implemented in the software *Regularity*. The signal-processing combines a global 2D-FT, column-wise 1D-FTs, a structure-tensor-based orientation analysis, and a phase continuity evaluation. As the method contains no trainable parameters, the results are, in principle,

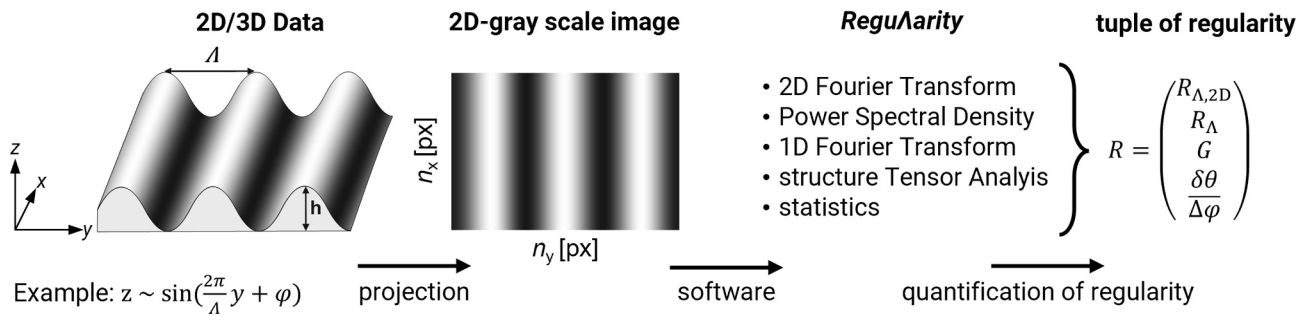


Fig. 1. Deterministic workflow for the quantification of structural regularity using *ReguAriaty*. Surface data (2D/3D topography or intensity) are projected into grey-scale images, which are processed by the software using spectral, statistical, and tensor-based methods. Regularity is described by a five-dimensional tuple $R = (R_{\Lambda,2D}, R_\Lambda, G, \delta\theta, \Delta\phi)$, capturing global and local variations in spatial periodicity, orientation, and phase continuity.

reproducible across datasets and instruments given identical inputs and configurations.

Starting from 2D/3D surface data – typically describing a grating-like periodic pattern – the images are projected into grey-scale images. These are then processed by a combination of spectral, statistical, and tensor-based methods to extract structural information. Central to this approach is the characterization of regularity via a five-dimensional descriptor, the regularity tuple.

$$R = (R_{\Lambda,2D}, R_\Lambda, G, \delta\theta, \Delta\phi) \quad (1)$$

This tuple systematically encodes critical aspects of structural regularity: global and local variation in spatial periodicity, spatial homogeneity, orientation, and phase continuity. The subsequent sections describe the individual computational steps in detail.

The core of the method lies in the application of Fourier analysis for extracting spatial frequency information that characterizes the periodicity of surface structures. *ReguAriaty* implements both global and local variants of the discrete Fourier Transform (FT). In the two-dimensional case, the entire microscopic image is transformed according to the 2D-FT, which is defined as

$$F(k_x, k_y) = \sum_{x=0}^{N_x-1} \sum_{y=0}^{N_y-1} f(x, y) \cdot e^{-i2\pi \left(\frac{k_x x}{N_x} + \frac{k_y y}{N_y} \right)}, \text{ with } k_x, k_y \in \left[-\frac{N}{2}, +\frac{N}{2} - 1 \right] \quad (2)$$

for a given two-dimensional signal $f(x, y)$ of dimension $N_x \times N_y$. Accuracy of the Fourier-based analysis is ensured by the following pre-processing steps: First, the mean grey-scale intensity is subtracted from the image to suppress the so-called DC component and to enhance the relative contrast of periodic features. Secondly, to reduce discontinuities in the context of Fourier transformations (e.g., the edges of the image or typical scale bars in microscopic images), a two-dimensional Hann-window $W(x, y)$ is applied.

$$W(x, y) = w(x) \cdot w(y) \quad (3)$$

It is defined as the product of two one-dimensional Hann-window functions $w(x)$ and $w(y)$ in x - and y -direction, respectively [43].

$$w(x) = \frac{1}{2} \left(1 - \cos\left(\frac{2\pi x}{N-1}\right) \right), w(y) = \frac{1}{2} \left(1 - \cos\left(\frac{2\pi y}{N-1}\right) \right) \quad (4)$$

Here, w is a continuous function with an amplitude ranging between 0 and 1 and N is a positive integer that represents the number of image pixels in the corresponding direction.

With these preparations, *ReguAriaty* implements a global analysis approach based on the radial power spectral density (PSD) derived from the 2D-FT of the entire image. The PSD is calculated by squaring the magnitude of the 2D-FT and performing a radial averaging over

concentric bins of spatial frequency $k = \sqrt{k_x^2 + k_y^2}$. This implementation differs from conventional PSD approaches, which are performed along a single axis. The radial PSD in *ReguAriaty* integrates the spectral power over all directions, providing an orientation-independent measure of the global periodicity. This produces a one-dimensional PSD profile as a function of the magnitude of the spatial frequencies from which the dominant spectral component k_{dom} is determined. To ensure comparability, the corresponding global dominant spatial period is then calculated after normalization as $\hat{\Lambda}_{2D} = 1/k_{\text{dom}}$. In addition, with the use of a Lorentzian fit function $f = y_0 + a/[b^2 + (x - x_0)^2]$, the period variation $\Delta\Lambda_{2D}$ is estimated as the half-width of the dominant peak in the PSD. For this purpose, *ReguAriaty* can determine the spatial periods of periodic surface structures as $\Lambda_{2D} = \hat{\Lambda}_{2D} \pm \Delta\Lambda_{2D}$. This results in a concise representation of the regularity of the dominant periodicity $R_{\Lambda,2D}$ as a relative parameter, providing a global FT-based measure of periodic regularity.

$$R_{\Lambda,2D} \equiv \frac{\Delta\Lambda_{2D}}{\hat{\Lambda}_{2D}} \quad (5)$$

However, the reliability of the extracted spatial periodicities in the resulting regularity parameter $R_{\Lambda,2D}$ critically depends on the underlying Fourier spectrum. In practice the presence of spectral “artifacts”, e.g., due to defects in the surface pattern and superimposed redeposited ablation products, can lead to incorrect spatial frequency selection according to the highest amplitude. In *ReguAriaty* the peak search is therefore restricted to a spatial frequency window K , i.e., the radial PSD is only evaluated for $k \in K$ while spatial frequencies outside this range are excluded from peak detection. It should be noted that this analysis window does not modify amplitudes or phases. It merely excludes DC-near components and implausible, high spatial frequencies from the dominance criterion. Here, $K = [k_{\min}, k_{\max}]$ denotes an admissible spatial frequency interval in μm^{-1} . The user may exclude DC-near components by choosing $k_{\min} > 0$ and limit the search range to $k_{\max} \leq k_{\text{Nyq}}$, ensuring that the fundamental peak and its sidebands are fully included. The Nyquist frequency $k_{\text{Nyq}} = 1/2\Delta x$ represents the maximum frequency that can be distinctly resolved in a sampled signal and equals half the sampling frequency $1/\Delta x$.

The grey-scale image is then sliced along the y -axis into columns of equal width according to the P³S method of Takenaka et al. [32] to assess local variations of the surface parameters. The column width can be adjusted as desired, for a precise analysis of the regularity a width of 1 pixel (px) is recommended. Each column is then evaluated in various arithmetic operations, whereby the initial step consists of a discrete 1D-FT, performed in the desired spatial frequency window K . For each column with a total length of N pixels, it decomposes the associated image segment $f[x]$ into its constituent spatial frequencies $F[k]$:

$$F[k] = \sum_{n=0}^{N-1} f[x] \cdot e^{-i2\pi \frac{kn}{N}}, \text{ with } k \in [0, N-1] \quad (6)$$

A sorting algorithm is then used to evaluate the full set of N Fourier spectra. For this purpose, both spatial frequencies (+/-) with the highest amplitude are automatically determined to calculate their distance d in the frequency space. This leads to the local dominant spatial period $\Lambda_j = 2/d$ of a single column j [44]. Finally, the mean value $\bar{\Lambda}$ and the standard deviation $SD(\Lambda)$ of all dominant spatial periods Λ_j are used to calculate R_Λ , which is introduced here as a dimensionless measure of the regularity of the most frequent period. It represents the ratio of the variation $\Delta\Lambda$ of the most frequent period distribution of all Λ_j and its average value $\bar{\Lambda}$.

$$R_\Lambda = \frac{SD(\Lambda)}{\bar{\Lambda}} \equiv \frac{\Delta\Lambda}{\bar{\Lambda}} \quad (7)$$

Using Λ_j as a characteristic attribute of each individual image segment allows to calculate the Gini coefficient G . It considers absolute deviations between the columns and weights them linearly. This allows for a robust assessment of local regularity and its cumulative variation.

$$G = \frac{\sum_{i=1}^n \sum_{j=1}^n |\Lambda_{j+1} - \Lambda_j|}{2n \sum_{i=1}^n \Lambda_i} \quad (8)$$

In addition to the local and global 1D-FT/2D-FT regularity analysis, *Regularity* allows to determine the angular uniformity of structural alignment $\delta\theta$. Analogous to Gniliitskyi et al. [15], the calculation is performed based on the *ImageJ* plugin *Orientation J* [28,29]. Beyond this state of the art, *Regularity* combines the mathematical routine of *OrientationJ* with the fully automated evaluation of $\delta\theta$. This includes the calculation of the gradient $\nabla f(x)$, which indicates the direction of the steepest intensity increase at each pixel. The integration of $\nabla f(x)$ via an isotropic window function w (usually a Gaussian window function w) leads to the 2nd-order structural tensor $J(x_0)$.

$$J(x_0) = \int w(x - x_0) \nabla f(x) \nabla f(x)^\top dx \quad (9)$$

As the choice of gradient directly determines the quality and stability of the structural tensor, the gradient directly influences, e.g., the robustness to noise, the sensitivity to fine structures and the reliability of the subsequent orientation determination. Therefore, the calculation of the gradient was performed with a Riesz-filter $R_i(f(x))$, where $i \in \{1,2\}$ denotes the spatial directions x and y , respectively. This filter provides isotropic, rotation-invariant gradients and is chosen by its robustness and isotropy, thus justifying the increased computational effort [45].

$$R_i(f(x)) = F^{-1} \left[i \frac{k_i}{\|k\|} F(f(x)) \right], \text{ with } i \in \{1, 2\} \quad (10)$$

The isotropic window $w(x-x_0)$ also influences the calculation of the structural tensor. The window size σ determines the standard deviation of the local Gaussian window used to weigh the gradient in the structure tensor calculation.

$$w(x - x_0) = \frac{1}{2\pi\sigma^2} e^{-\frac{\|x - x_0\|^2}{2\sigma^2}} \quad (11)$$

Here, $\|x - x_0\|^2$ represents the squared Euclidean distance between a pixel x and the center position x_0 . This exponential decay ensures that pixels closer to the center contribute more strongly to the tensor than those further away. The parameter σ controls the spatial extent of this weighting: a smaller σ restricts the influence on a narrow neighborhood, enhancing spatial resolution but increasing noise sensitivity, while a larger σ leads to broader smoothing, improving noise robustness at the cost of resolution.

The eigenvalues and eigenvectors of the structural tensor $J(x_0)$ provide information about the local image structure. The eigenvector, which belongs to the largest eigenvalue, indicates the dominant orientation of the local image gradient. The corresponding angle θ is usually determined as follows:

$$\theta = \frac{1}{2} \arctan \left(\frac{2J_{12}}{J_{22} - J_{11}} \right) \quad (12)$$

The value of $\delta\theta$ is then half of the absolute difference between the two determined limiting angles θ_1 and θ_2 , which quantifies the angular spread across the structure and complements the spatial period analysis with a measure of directional coherence:

$$\delta\theta = \frac{|\theta_2 - \theta_1|}{2} \quad (13)$$

As a final component of the analysis, the phase of the dominant frequency component in each segment is evaluated to quantify phase regularity. Artifacts in the Fourier spectrum – such as surface defects or redeposited material – may distort amplitude-based selection but typically preserve phase information. The absolute difference between adjacent segments is calculated as:

$$\Delta\varphi = |\varphi_{j+1} - \varphi_j| \quad (14)$$

From this, the mean phase change $\bar{\Delta\varphi}$ and its standard deviation are derived, providing a scalar measure of local phase continuity and an additional indication of pattern stability.

All parameters are finally integrated into the five-dimensional regularity tuple, as defined in Eq. (1), which comprehensively characterizes the regularity of the evaluated periodic surface pattern in terms of spatial period variation, homogeneity, orientation, and phase distortions. This procedure promises a fast and systematic analysis, especially when computing a larger number of micrographs in efficient multi-threading processing. For clarity, Table 1 shows a summary of the five regularity parameters determined with *Regularity*.

3. Materials and methods

3.1. Sample preparation and generation of LIPSS

To demonstrate the capabilities of the developed software *Regularity*, a comparative analysis is carried out using LIPSS exhibiting varying degrees of regularity. As substrate materials, AISI 316L stainless

Table 1

Summary of the regularity parameters implemented in *Regularity*, including their mathematical symbols, analytical methods, and sensitivity to specific structural irregularities in laser generated periodic surface structures.

Regularity parameter	Symbol	Type of regularity	Sensitive to	References
Regularity of 2D-period	$R_{\Lambda,2D}$	Spread of all LIPSS periods	Global superposition of multiple periodicities, structural disorder	[6,27]
Regularity of period	R_Λ	Spread of most frequent LIPSS periods	Local defects, abrupt period changes, outliers	[32]
Gini coefficient	G	Homogeneity of period distribution	Subtle non-uniformities, cumulative distribution effects	[14,30,31]
DLOA	$\delta\theta$	Angular uniformity of structural alignment	Local curvature of LIPSS ridges	[15,27]
Regularity of phase	$\Delta\varphi$	Local phase continuity along structure orientation	Local defects, disruptions, bifurcations	[32]

steel and AlMg5 aluminum alloy were selected, both known to exhibit markedly different ability to form regular LIPSS pattern [15,46]. This originates from differences in the thermo-physical properties of the two distinct alloys, affecting ablation processes following the ultrafast laser excitation. In preparation for the subsequent laser structuring, the AISI 316L and AlMg5 sample plates (10×10 mm 2) were ground and then polished with a resulting average surface roughness of $S_a < 10$ nm. A sample preparation system (EcoMet300/ AutoMet300 Buehler, ITW, Test & Measurement GmbH, Germany) was utilized for this purpose using 300 to 1200 grit SiC paper. Finally, the AISI 316L sample surfaces were polished with 9 µm, 3 µm and 1 µm polycrystalline diamond suspension. The polished samples were ultrasonically cleaned in acetone and isopropanol for 10 min prior to laser structuring.

Low-spatial frequency LIPSS of type I (LSFL-I) [47] were generated using previously optimized processing parameters and the experimental setup depicted in Fig. 2. The ultrashort, pulsed laser beam with a wavelength of $\lambda = 1025$ nm, a pulse duration of $\tau = 300$ fs and a repetition frequency of $f_{rep} = 100$ kHz was delivered by a commercial fs-laser system (JenLas D2.fs, Jenoptik, Germany) and expanded by a telescope. A galvanometer scanner (IntelliScan, Scanlab, Germany) with a f-theta lens (JENar, Jenoptik, Germany) was used to focus the Gaussian laser beam (focal length $f_L = 100$ mm, focal spot diameter $2w_0 \sim 24$ µm) and for its relative movement. The scanning direction was set perpendicular to the linear beam polarization to promote maximal structural regularity [22].

On AISI 316L, a scanning velocity of $v = 0.6$ m/s, a hatch distance of $\Delta x = 6$ µm and a peak fluence of $F_0 = 1.2$ J/cm 2 were employed in accordance with Lubig et al. [12]. For AlMg5, $v = 0.3$ m/s, $\Delta x = 3$ µm and $F_0 = 0.3$ J/cm 2 were determined as the set of parameters.

3.2. Software implementation and algorithmic procedure

Regularity was developed in Python 3.11 within the integrated development environment (IDE) Spyder. The implementation relies on common open-source packages, including, e.g., NumPy (v1.26), SciPy (v1.13), PyQt5 (v5.15) for the graphical user interface as well as OpenCV (v4.9) for image processing and Matplotlib (v3.9) for data visualization. The entire computational procedure is summarized in Fig. 3, which outlines the sequence of preprocessing, global and local Fourier analysis, orientation evaluation, and phase quantification that jointly define the five-dimensional regularity tuple R (Eq. (1)).

3.3. Analysis of regularity

Micrographs of LIPSS on both materials were obtained with a scanning electron microscope (EVO 40, Carl Zeiss AG, Germany) and evaluated in comparison with an idealized, artificially generated sinusoidal grey-scale pattern of comparable spatial periodicity. These three surface patterns serve as representative cases for subsequent comparative regularity analysis, in which two distinct evaluation methods are applied. First, in Sec. 4.1, the regularity is assessed using a manual approach based on conventional two-dimensional Fourier analysis (as implemented in the software *Gwyddion* [48]) and on directional orientation mapping using the *ImageJ*-Plugin *OrientationJ* [15,28,29]. This provides reference values for the dominant global spatial period $\hat{\Lambda}_{2D}$ and angular dispersion $\delta\theta$. In Sec. 4.2, the same surface data are analyzed using the software *Regularity* developed here. In contrast to the manual procedure, *Regularity* performs a fully automated, multi-parametric regularity analysis (Fig. 1). For reproducibility, the annotations of the micrographs were erased using the ROI-selector. The admissible spatial frequency domain was set to $K \in [0.1, 6.2 = k_{Nyq}] \mu\text{m}^{-1}$, which equals periods in the range of $\Lambda = 0.16$ µm to $\Lambda = 10$ µm. Detailed instructions on how to use the versatile features of the software can be found on GitHub (<https://github.com/fs-eracr/Regularity>). Designed for high-throughput analysis, *Regularity* allows for the fully automated evaluation of large image datasets, limited only by the computing resources available. Benchmark tests demonstrated a reliable analysis of 50 images (1024 × 690 pixels) on a standard PC equipped with 32 GB RAM and a 1.7 GHz Intel Core Ultra 7 processor within 90 s. *Regularity* implements two complementary analysis modules: **Segment & Compute** (S&C), based on Fourier analysis, and **DLOA**, based on structure tensor evaluation (see Fig. 4). Both methods are parameterizable and can be applied independently or jointly, provided that consistent settings are used across the entire dataset. To initiate the analysis process, it is necessary to specify the directory path that contains the images intended for examination. The subsequent step is to store the physical dimensions of the images. For this purpose, the µm/px ratio is calculated based on the physical image dimensions and resolution, which has a direct influence on the following calculation of the structure period Λ .

After choosing one of the mentioned methods, *Regularity* allows defining a region of interest (ROI) to exclude image artefacts such as scale bars or annotations as shown in Fig. 5a. In the case of the S&C method, *Regularity* computes the global spatial frequency distribution of the entire image via 2D-FT. By radial averaging of the resulting PSD, the dominant global spatial period $\hat{\Lambda}_{2D}$, its spectral width $\Delta\Lambda_{2D}$, and the corresponding global regularity measure $R_{\Lambda,2D}$ are extracted using a

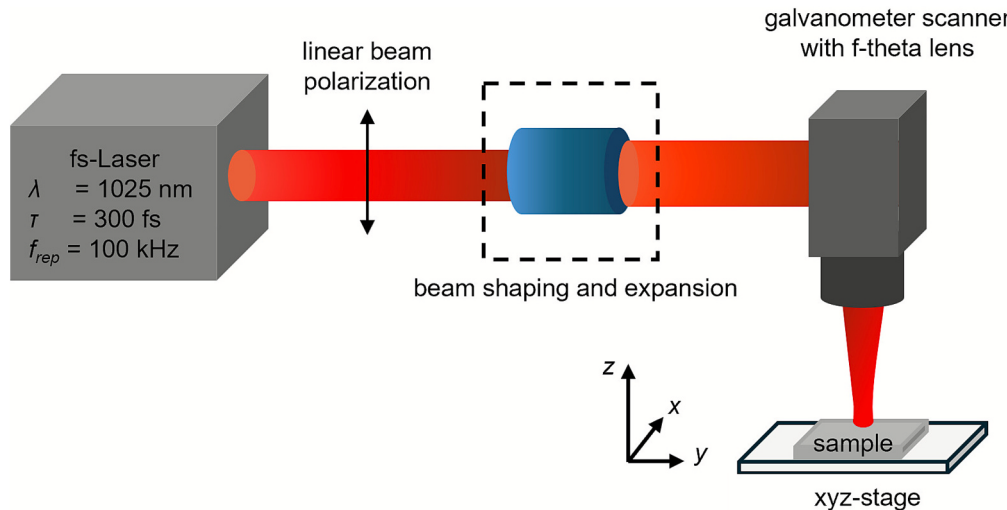


Fig. 2. Scheme of the laser processing setup used to generate LIPSS at the surface of AISI 316L stainless steel and AlMg5 aluminum alloy.

```

Input: grey-scale microscopy image I(x, y)

Output: Regularity tuple R = (RA, 2D, RA, G, δθ, ⟨|Δφ|⟩)

Preprocessing

- Optional: Subtract mean intensity
- Optional: Apply Hann window

Step 1: Global Fourier analysis

- Compute 2D-FFT → radial PSD
- Fit Lorentzian Peak → Λ2D, ΔΛ2D
- Compute RA,2D = ΔΛ2D/Λ2D

Step 2: Local Fourier analysis

- For each column ⊥ to ridges:
  Compute 1D-FFT → Λj, φj
- Compute RA = SD(Λj)/mean(Λj)
- Compute Gini coefficient G from {Λj}

Step 3: Orientation analysis

- Compute structure tensor J(x0)
- Extract orientation distribution
- Determine δθ/DLOA

Step 4: Phase analysis

- Compute Δφj = φj+1 - φj
- Compute ⟨|Δφ|⟩

Return: R = (RA,2D, RA, G, δθ, ⟨|Δφ|⟩)

```

Fig. 3. Pseudo-code of the computational procedure used in *Regularity*.

Lorentzian fit to the PSD peak. Subsequently, the S&C method performs a pixel-wise segmentation of the image into columns, each of which is subjected to a 1D-FT. This yields the dominant spatial period Λ_j for each column segment. From the ensemble of all local values, the mean period $\bar{\Lambda}$, the standard deviation $SD(\Lambda)$, and the resulting local regularity parameter R_A are computed. To further characterize the spatial homogeneity of the periodic structure, the Gini coefficient G is derived from the distribution of all Λ_j . This metric quantifies the cumulative deviation in segment-wise periodicity, offering a sensitive measure of pattern uniformity and homogeneity. Finally, the inter-segment phase distribution is assessed. From the phase ϕ_j of the dominant frequency in each segment, the software calculates the mean inter-segment phase deviation $\overline{\Delta\phi}$ along with its standard deviation. This parameter captures continuity or disruption in the phase of the pattern across the image. Optionally, the gradient-based module computes the Dispersion of the LIPSS Orientation Angle $\delta\theta$ using a Riesz-filter-based structural tensor can be started via the DLOA method and choosing an ROI.

The full set of regularity parameters and corresponding statistical descriptors is summarized in a result window (Fig. 5b) and can be exported as an.xlsx-file for storage and further data processing. All images, including the 2D-FT spectra, the normalized PSD, as well as the period and phase graphs, are organized in a data browser that opens automatically as a table. For clarity, the values corresponding to the regularity tuple $R = (R_{A,2D}, R_A, G, \delta\theta, \overline{\Delta\phi})$ according to Eq. (1) are displayed at the top of the results table in bold letters.

3.4. Robustness assessment of regularity analysis

Robustness against varying the ROI size, the range of K and the grey-scale contrast of the underlying micrographs was evaluated, while keeping pre-processing (DC background subtraction, 2D Hann window). The position of the selected ROI within the micrograph and structure-tensor parameters were kept constant across all perturbations to isolate the effect of ROI size, K , and image contrast. For each of the

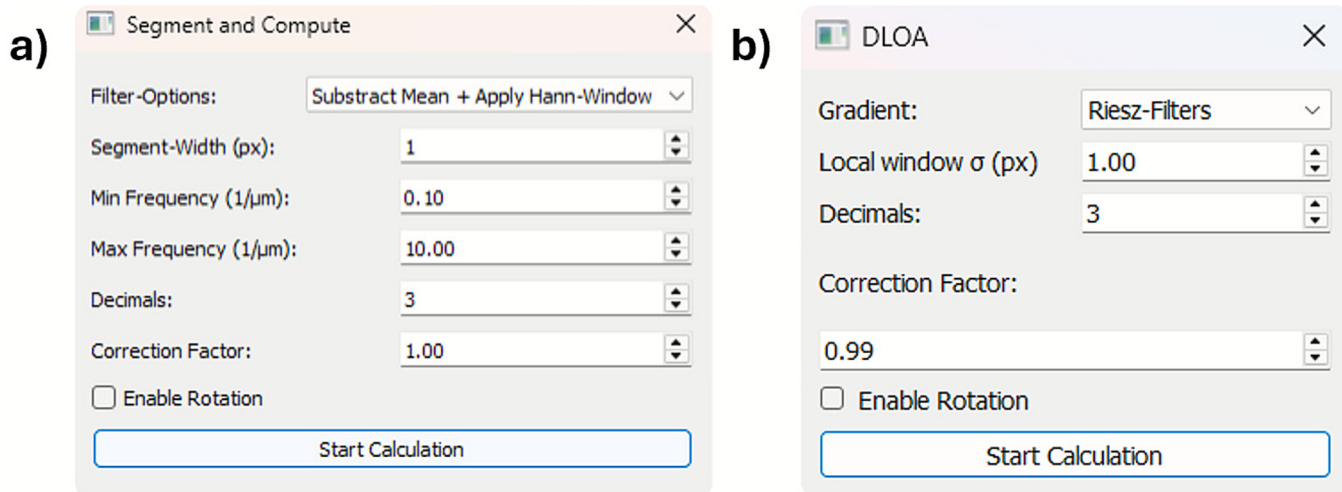


Fig. 4. Default set of parameters used for the calculations: a) Segment & Compute (S&C) and b) calculation of $\delta\theta$ (DLOA).

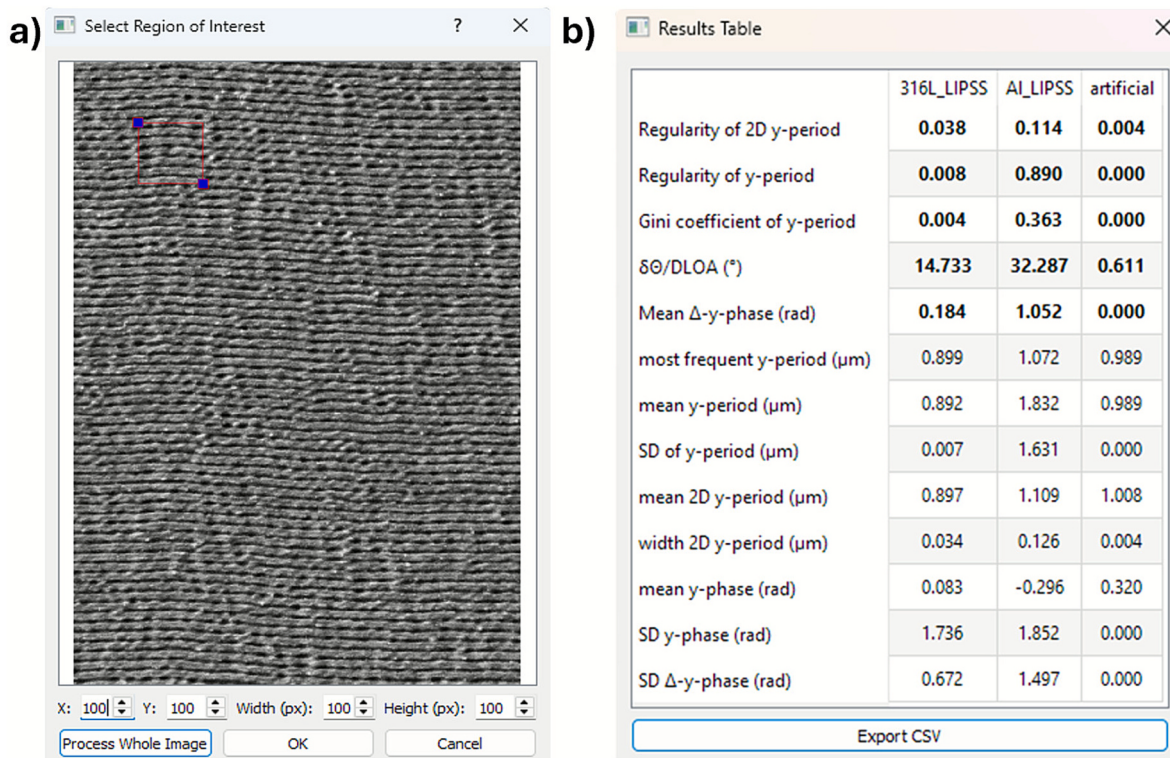


Fig. 5. GUI of ReguAarity: a) Selection of the region of interest (ROI) within the investigated image and b) output window tabulating the results of the regularity measures that can afterwards be exported as a.xlsx-file.

following configurations, we computed $\hat{\Lambda}_{2D}$, $\Delta\Lambda_{2D}$ and $\delta\theta$ and reported absolute values:

- The ROI size was varied from the entire usable image size (ROI = 1) down to a quarter of the image (ROI = 0.25) by preparing centered crops using ReguAarity.
- The peak selection was probed with four different admissible spatial frequency domains $K \in \{[0.0, 6.2 = k_{Nyq}] \mu\text{m}^{-1}, [0.1, 0.6] \mu\text{m}^{-1}, [0.5, 1.5] \mu\text{m}^{-1}, [0.8, 1.2] \mu\text{m}^{-1}\}$.
- Global linear contrast scaling was applied with the native Windows image editor (*Windows Photo App*) to scale the contrast from -100 % to + 100 %.

4. Experimental results

4.1. Manual analysis of LIPSS regularity

A 2D-FT analysis of the grey-scale images in Fig. 6 with Gwyddion (v2.69) led to global spatial periods that were determined to be $\Lambda_{2D} = (0.91 \pm 0.02) \mu\text{m}$ for AISI 316L (Fig. 6a), $\Lambda_{2D} = (1.04 \pm 0.21) \mu\text{m}$ for AlMg5 (Fig. 6b) and $\Lambda_{2D} = (0.99 \pm 0.01) \mu\text{m}$ for the artificial test pattern (Fig. 6c). Cross-sectional profiles of the features were extracted from the 2D-FT spectra (Fig. 6d-f) and are displayed below the corresponding 2D-FTs (Fig. 6g-i). The position and the full-width-at-half-maximum (FWHM) of the peaks were then measured manually using a Lorentzian fit function.

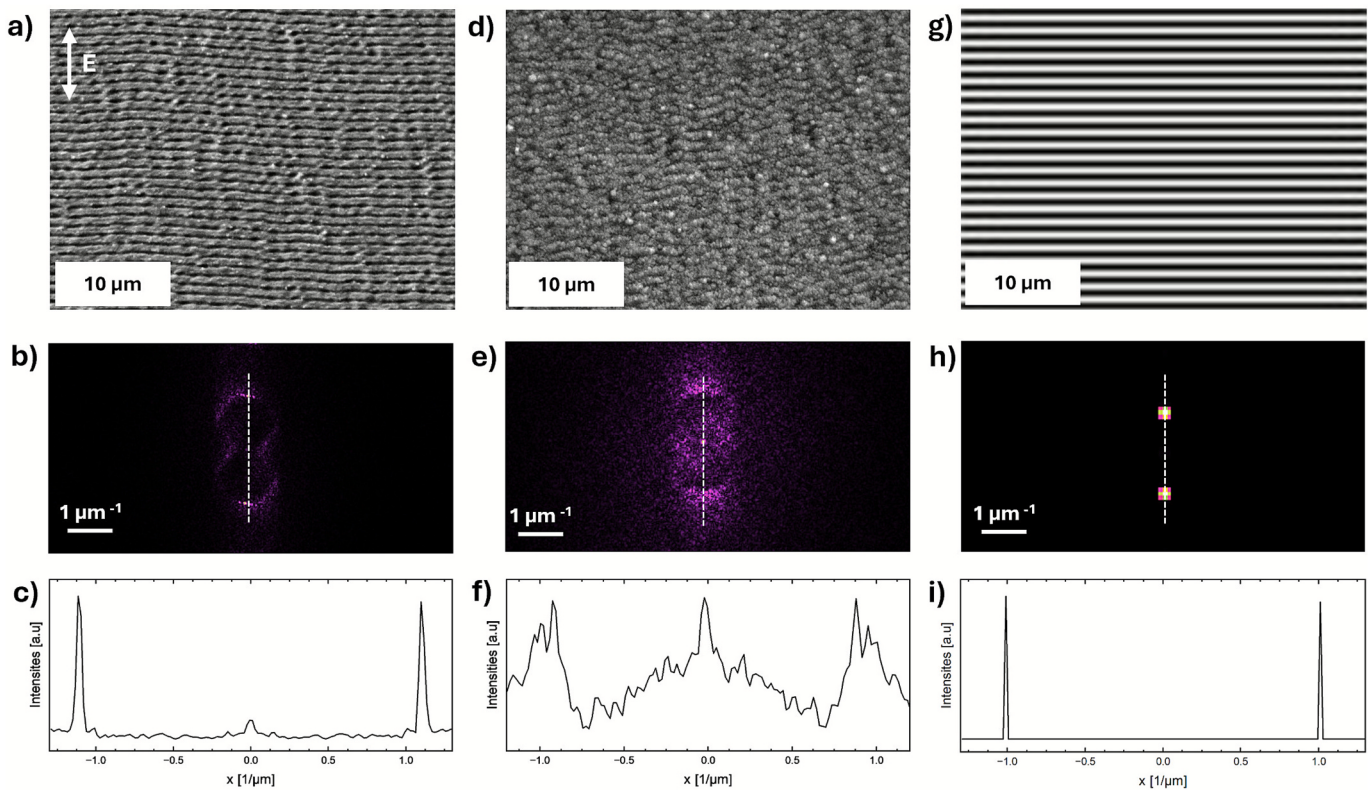


Fig. 6. Regularity analysis of periodic surface patterns. The microscopic images (top row) serve as the basis for computing the 2D-FT spectra (middle row) and for subsequently evaluating the corresponding spectral cross sections (bottom row) taken along the white dashed lines. The analysis compares LIPSS generated on AISI 316L stainless steel (a-c) and on AlMg5 aluminum alloy (d-f) with an ideal, artificially generated sinusoidal grey-scale pattern (h-j). LIPSS were produced using linear beam polarization, with the polarization direction indicated by the arrow in (a).

The magnitude of the specified variation range provides insight into the spatial periods present on the surface, thereby indicating the regularity of the LIPSS. In the case of AISI 316L stainless steel (Fig. 6a–c), the global dominant spatial period in the entire image is $\hat{\Lambda}_{2D} = 0.91 \mu\text{m}$, with a range of $\Delta\Lambda_{2D} = \pm 0.02 \mu\text{m}$ of the observed values. In contrast, the obviously lower regularity of LIPSS on AlMg5 alloy (Fig. 6d–f) is expressed in a significantly broader variation range of the spatial period of $\Delta\Lambda_{2D} = \pm 0.21 \mu\text{m}$ around the global dominant spatial period $\hat{\Lambda}_{2D} = 1.04 \mu\text{m}$. Although the artificial profile (Fig. 6g–i) represents a mathematically perfect sinusoidal modulation, the resulting peak in the Fourier intensity profile appears slightly broadened, with a fitted value of $\Delta\Lambda_{2D} = \pm 0.01 \mu\text{m}$. This broadening can be attributed to the finite image size, pixel discretization, and spectral leakage effects inherent to the Fourier transform of windowed spatial data.

The angular alignment and local curvature of the surface structures, serving as an additional measure of regularity, was evaluated manually using *OrientationJ* following the procedure proposed by Gnilitskyi et al. [15]. By applying a Riesz filter as a gradient operator and a local window size of $\sigma = 1 \text{ px}$, the corresponding values of $\delta\theta$ were determined to be $\delta\theta = 11.5^\circ$ for AISI 316L, $\delta\theta = 23^\circ$ for AlMg5 and $\delta\theta = 1^\circ$ for the artificial profile. The values are comparable with the experiments of Gnilitskyi et al. [15], who reported $\delta\theta = 9.2^\circ$ for steel and $\delta\theta = 26.7^\circ$ for aluminum. The increased $\delta\theta$ value for AISI 316L in the current study compared to the ideal sinusoidal grating can be attributed to a moderate waviness of the LIPSS in the horizontal direction. The nearly twofold increase for AlMg5 results from local variations in structural orientation and local LIPSS curvature, which is accompanied by numerous bifurcations of the LIPSS ridges.

4.2. Surface analysis using the ReguAriaty software

The quantification of the regularity of the artificial sinusoidal reference pattern (Fig. 6g) as a benchmark of ideal structural order using the software *ReguAriaty* is summarized in Table 2 in comparison with the laser-generated LIPSS pattern. The global spatial period of the reference pattern is determined as $\hat{\Lambda}_{2D} = 1.008 \mu\text{m}$ with a spectral width of $\Delta\Lambda_{2D} = 0.004 \mu\text{m}$, resulting in a global regularity parameter of $R_{\Lambda,2D} = 0.004$ according to Eq. (5). Locally the mean period of the evaluated segments is $\bar{\Lambda} = 0.989 \mu\text{m}$ with a standard deviation of $SD(\Lambda) = 0$, confirming $R_\Lambda = 0$ and $G = 0$. The calculation of DLOA results in a very small value of $\delta\theta = 0.61^\circ$. The observed deviation from zero arises from the discrete nature of the determination of the orientation spectrum and can, therefore, be taken as the measurement uncertainty associated with DLOA analysis. The ideal regular geometry is further reflected in the phase analysis, which also yields zero for the mean inter-segment phase differences $\bar{\Delta}\phi$ (Eq. (14)), emphasizing phase uniformity across the entire

Table 2

Regularity parameters of the artificial sinusoidal test pattern and of LIPSS on AISI 316L and AlMg5 determined with the software *ReguAriaty*.

parameter	artificial test pattern	LIPSS on AISI 316L	LIPSS on AlMg5
$R_{\Lambda,2D}$	0.004	0.038	0.114
R_Λ	0	0.008	0.890
G	0	0.004	0.363
$\delta\theta [\circ]$	0.61	14.73	32.29
$\bar{\Delta}\phi[\text{rad}]$	0	0.184	1.052
$\hat{\Lambda}_{2D} [\mu\text{m}]$	1.008	0.897	1.109
$\Delta\Lambda_{2D} [\mu\text{m}]$	0.004	0.034	0.126
$\bar{\Lambda} [\mu\text{m}]$	0.989	0.892	1.832
$SD(\Lambda) [\mu\text{m}]$	0	0.007	1.631

surface pattern. This confirms that *Regularity* correctly identifies the perfect structural periodicity and regularity of the reference, thus validating the sensitivity and accuracy of the software. Deviations from ideal values arise solely from discretization and floating-point limits and define the instrumental resolution baseline.

Using the example image of LIPSS on AISI 316L (Fig. 6a–c), Fig. 7 illustrates the set of graphs generated and stored within the data browser during the analysis process. These include the pre-processed grey-scale image with the Hann-window applied and the DC component removed (Fig. 7a), the corresponding 2D-FT spectrum (Fig. 7b), the orientation spectrum obtained from the DLOA analysis (Fig. 7c) and the spatial period and phase profiles calculated segment-wise (Fig. 7d). All visualizations can be separately saved as image files. The plots are interactively scalable and, via the integrated export function, can be used for further evaluation and processing. For this purpose, the underlying plot data are automatically exported as an Excel spreadsheet to the specified output directory. The corresponding quantitative analysis summarized in Table 2 reveals a slightly reduced but still high degree of regularity of LIPSS on AISI 316L. In this case, the global dominant spatial period is extracted as $\hat{\Lambda}_{2D} = 0.897 \mu\text{m}$ with a spectral width of $\Delta\Lambda_{2D} = 0.034 \mu\text{m}$, yielding $R_{\Lambda,2D} = 0.038$. This agrees well with the manually determined value of $\Lambda_{2D} = (0.91 \pm 0.02) \mu\text{m}$, measured via Lorentzian fitting of the 2D-FT profile. The local periodicity parameters are also characterized by a high degree of local regularity. *Regularity* identifies a dominant local

period of $\bar{\Lambda} = 0.892 \mu\text{m}$, with a standard deviation of $\text{SD}(\Lambda) = 0.007$, resulting in a normalized variation of $R_{\Lambda} = 0.008$. These values indicate a very low variation of local periodicity, which is statistically corroborated by the Gini coefficient of $G = 0.004$. The calculated value of $\delta\theta = 14.73^\circ$ is in good agreement with the manually obtained value of $\delta\theta = 11.5^\circ$. The slight deviation results from the objective analysis, which, unlike manual analysis, is not based on subjective thresholds. The analysis of phase regularity reveals a mean inter-segment deviation of $\Delta\varphi = 0.184 \text{ rad}$, indicating the presence of mild phase drift but no major structural bifurcation. Overall, the irradiation of AISI 316L with the given processing conditions yields highly regular LIPSS with excellent agreement of the regularity parameters obtained from manual and automated analysis, validating both the fidelity and robustness of *Regularity*.

The LIPSS on AlMg5 (Fig. 6b), in contrast, show pronounced irregularity across all parameters (Tab. 2). *Regularity* determines a global period of $\hat{\Lambda}_{2D} = 1.109 \mu\text{m}$ with a very broad spectral width of $\Delta\Lambda_{2D} = 0.126 \mu\text{m}$, corresponding to a higher global regularity index of $R_{\Lambda,2D} = 0.114$. This matches the manual analysis with a spatial period of $\Lambda_{2D} = (1.04 \pm 0.21) \mu\text{m}$, although the manual analysis reveals a larger variation range of the spatial periods due to the manually chosen borders of the fit. Segment-wise, the local dominant period is $\bar{\Lambda} = 1.83 \mu\text{m}$ with $\text{SD}(\Lambda) = 1.631 \mu\text{m}$ leading to a remarkably increased irregularity value of $R_{\Lambda} = 0.89$. The Gini coefficient increases strongly to $G = 0.363$,

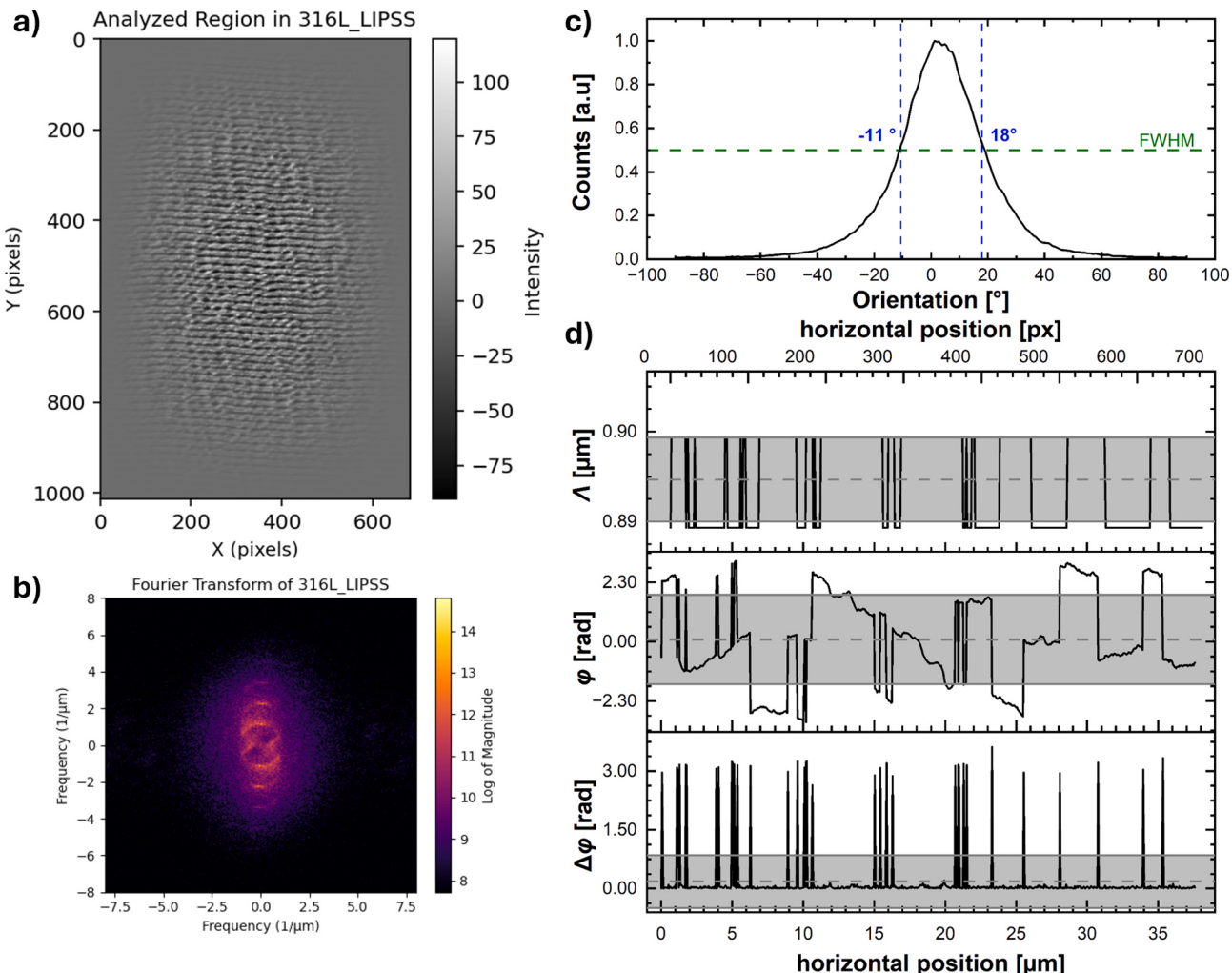


Fig. 7. Surface evaluation with *Regularity* using the example of LIPSS on AISI 316L: a) pre-processed grey-scale image with applied Hann window and removed DC-component, 2D Fourier transform of the SEM image, c) LIPSS orientation spectrum, and d) distribution of spatial periods and phase information, both computed for each column after segmentation of the image. The dotted lines in (d) correspond to the mean values, and the grey-shaded zones illustrate the standard deviation.

reflecting significant spatial variation and the presence of pronounced outliers. Orientation analysis reveals a DLOA value of $\delta\theta = 32.29^\circ$, consistent with the observable well-pronounced curvature, bifurcations, and the non-uniform ridge alignment in Fig. 6d. Consequently, the phase deviation $\Delta\phi = 1.052$ rad indicates considerable inter-segment incoherence. Altogether, AlMg5 alloy proves to be a substrate prone to generating highly irregular LIPSS under the applied conditions.

These findings illustrate that the five-dimensional regularity tuple R provides a suitable set of parameters for the quantitative analysis of different surface morphologies. While the ideal sinusoidal reference confirms the internal consistency and sensitivity of the implemented algorithms, the comparative evaluation of AISI 316L and AlMg5 alloy highlights the practical benefit of *Regularity* in capturing relevant variations in experimentally generated structures.

4.3. Robustness assessment of the regularity tuple R

4.3.1. Influence of the ROI area

The evaluation of the influence of the ROI area in Fig. 8a demonstrates the stability of the parameters $\hat{\Lambda}_{2D}$, $\Delta\Lambda_{2D}$ (given by the error bars of $\hat{\Lambda}_{2D}$ in Fig. 8) and $\delta\theta$ calculated for the artificial test pattern (Fig. 6g), thereby highlighting the robustness of the algorithm under ideal conditions. For experimentally generated LIPSS patterns (Fig. 6a,d), the robustness analysis exhibits different behavior, which can be attributed to the material-dependent deviations in regularity already observed visually. This observation underlines the need to select a suitable ROI

size.

In the case of regular LIPSS on AISI 316L, all regularity parameters remain almost stable across the investigated ROI area range, except for $\Delta\Lambda_{2D}$, which is underestimated for the smallest ROIs. The underestimation arises from the reduced number of recorded spatial periods, which amplifies window and leak effects and thereby leads to an apparent period fluctuation. For the more irregular LIPSS on AlMg5, a significantly stronger dependence on the ROI area can be observed. Along with the reduced number of periods analyzed, small ROIs lead to an underestimation of $\hat{\Lambda}_{2D}$ and $\Delta\Lambda_{2D}$, with both metrics stabilizing only for sufficiently large ROIs. In addition, low-frequency artefacts have a greater influence on the automated selection of the dominant spatial frequency. In agreement with previous studies using *ImageJ/OrientationJ*, $\delta\theta$ stabilizes for both materials as the ROI area increases [15].

The results demonstrate that ROIs that are too small can systematically distort both the dominant spatial period and its corresponding variation. For the analysis of laser-induced periodic structures, the largest possible ROI should therefore be selected. Nevertheless, comparative studies with *Regularity* are still feasible for a given ROI size, as the same parameters are applied to all images simultaneously.

4.3.2. Influence of spatial frequency window size K

The analysis of the influence of the spatial frequency window K (Fig. 8b) confirms for the artificial sinusoidal reference pattern that the automated extraction of the period $\hat{\Lambda}_{2D}$ is highly robust as long as the frequency window fully encompasses the fundamental peak. For the

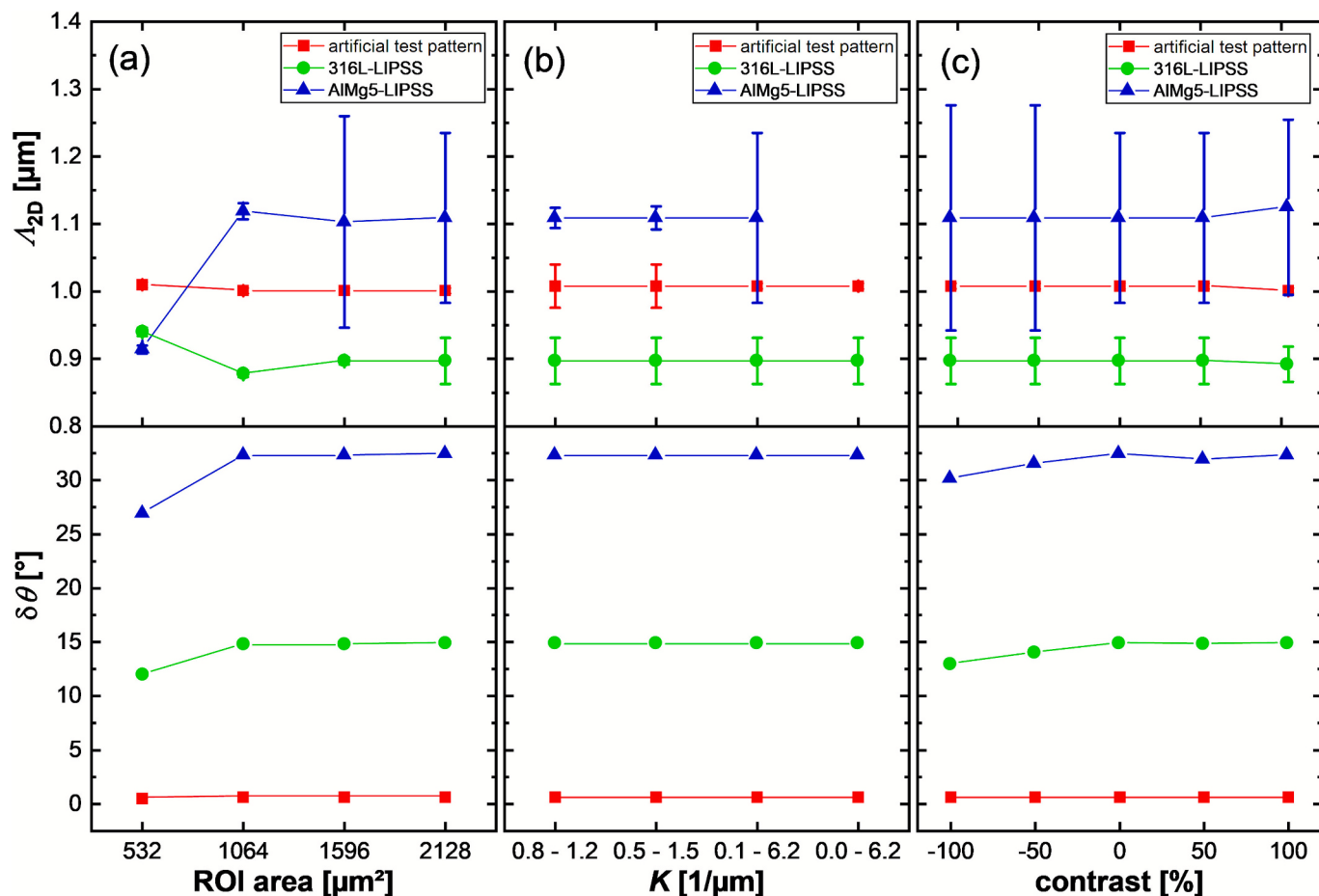


Fig. 8. Investigation of robustness of the regularity parameters $\hat{\Lambda}_{2D}$, $\Delta\Lambda_{2D}$ (given by the error bars of $\hat{\Lambda}_{2D}$), and $\delta\theta$ against variation of (a) ROI area, (b) spatial frequency window size K , and (c) global image contrast during the analysis of LIPSS on AISI 316L stainless steel (Fig. 6a; green circles), LIPSS on AlMg5 alloy (Fig. 6b; blue triangles) and the artificial sinusoidal reference pattern (Fig. 6c; red squares). (For interpretation of the references to colour in this figure legend, the reader is referred to the web version of this article.)

LIPSS patterns, however, reliable evaluation shows a pronounced dependence on K . Particularly for AlMg5, low-frequency artefacts appear in the Fourier spectrum (Fig. 6e), which enter the analysis when the selected interval K is too broad. If high-intensity components close to the DC-signal are located within the selected window, the PSD broadens and peak switching might occur, i.e., the automatically selected maximum can switch to spatial frequencies of the artefacts. In these cases, the software selects a spatial frequency that is not physically meaningful and is therefore excluded from the robustness analysis (see $K = [0.0\text{--}6.2] \mu\text{m}^{-1}$ for the blue curve in Fig. 8b).

Conversely, very narrow windows centered near the expected fundamental frequency truncate the peak flanks. This systematically underestimates $\Delta\Lambda_{2D}$ and can distort the determination of $\hat{\Lambda}_{2D}$ due to the limited adjustment. Spatial frequency windows that fully capture the fundamental peak, including its flanks, while suppressing low-frequency artefacts and higher harmonics, provide the most stable and plausible results and show the closest agreement with manual reference analyses. The results indicate that the selected range of spatial frequency K should be specified together with the regularity parameters.

4.3.3. Influence of global image contrast

When varying the global image contrast, the dominant period $\hat{\Lambda}_{2D}$ within the analyzed region remains nearly constant (Fig. 8c). The contrast has only a minor influence on the automated selection of $\hat{\Lambda}_{2D}$ itself. Only $\Delta\Lambda_{2D}$ shows slight changes with contrast, especially for LIPSS on AlMg5, where very high or very low contrasts lead to an overestimation of the width. In these cases, individual peaks of the modulated surface topography in the image are no longer clearly separable, giving the impression of increased structural irregularity. The contrast study confirms that, due to the linear nature of the Fourier transform, a global linear contrast change in the output image only rescales frequency amplitudes and strengthens the DC component without altering peak positions. As long as the basic structures of the pattern are not suppressed by excessive contrast reduction, $\hat{\Lambda}_{2D}$ and $\Delta\Lambda_{2D}$ remain virtually unaffected.

The orientation dispersion $\delta\theta$ proves to be largely robust under moderate contrast variations, showing only marginal effects that become discernibly at very low contrast levels. This results from reduced pixel-intensity differences, which make finer structural gradients undetectable. The contrast setting only becomes critical when clipping occurs, i.e., saturation at the upper and lower limits of the dynamic range, which truncates pixel intensities. Intensity gradients are then flattened or replaced by artificial step edges, broadening the distribution of local orientations and increasing $\delta\theta$. Under conditions without clipping, the regularity results obtained for the sinusoidal reference pattern and the LIPSS on AISI 316L remain stable within numerical dispersion, while a slightly greater sensitivity of $\delta\theta$ is observed for LIPSS on AlMg5. This is due, on the one hand, to superimposed particles and, on the other hand, to higher structural irregularity. Overall, the contrast study thus demonstrates that global linear contrast scaling is uncritical for regularity analysis as long as clipping is avoided and essential structural image information is preserved, whereas extreme contrasts may lead to an overestimation of the period width and orientation dispersion, particularly in complex and irregular patterns.

5. Conclusion

In this work, we introduced *Regularity*, a novel software tool for the objective, fully automated characterization of the regularity of periodic surface patterns based on microscopy images. Central to this contribution is the conceptual advancement of a five-parameter regularity tuple – comprising the spread of the 2D period $R_{\Lambda,2D}$, the regularity of the spatial period R_Λ , the Gini coefficient G , the Dispersion of the LIPSS Orientation Angle $\delta\theta$ (DLOA), and the average phase deviation $\bar{\Delta}\varphi$. Each parameter encodes a distinct morphological descriptor of surface

morphological order and disorder, providing a comprehensive, physically grounded quantification of pattern regularity. This multi-parametric framework provides a useful contribution to surface engineering and materials science, where the functionality of laser-structured surfaces – ranging from tailored wettability and friction to enhanced optical, biological, or tribological behavior – critically depends on the regularity and periodicity of surface features. By allowing unbiased, reproducible, and scalable assessment of structural quality across different material classes and imaging modalities, *Regularity* supports the rational design of laser-based functional surfaces. The demonstrated application to both idealized test patterns and experimentally generated LIPSS on metallic substrates (AISI 316L steel and AlMg5 aluminum alloy) validates the robustness and interpretability of the approach. Beyond its functionality in comparative LIPSS analysis, the software is designed for high-throughput processing, addressing the growing demand for data-driven surface optimization in the context of machine learning and digital materials design. Thus, *Regularity* contributes to the standardization and acceleration of regularity assessment in laser material processing and fosters the systematic development of next-generation functional surfaces.

Declaration of Generative AI and AI-assisted technologies in the writing process

During the preparation of this work the authors used ChatGPT to improve readability and language. After using this tool, the authors reviewed and edited the content as needed and take full responsibility for the content of the published article.

CRediT authorship contribution statement

Eric Rahner: Writing – review & editing, Writing – original draft, Visualization, Validation, Software, Methodology, Investigation, Formal analysis, Data curation, Conceptualization. **Tobias Thiele:** Writing – review & editing, Writing – original draft, Visualization, Validation, Software, Methodology, Investigation, Formal analysis, Data curation, Conceptualization. **Heike Voss:** Writing – review & editing, Writing – original draft, Visualization, Validation, Software, Methodology, Investigation, Formal analysis, Data curation, Conceptualization. **Frank A. Müller:** Writing – review & editing, Writing – original draft, Visualization, Validation, Software, Methodology, Investigation, Formal analysis, Data curation, Conceptualization. **Jörn Bonse:** Writing – review & editing, Writing – original draft, Visualization, Validation, Supervision, Software, Project administration, Methodology, Investigation, Funding acquisition, Formal analysis, Data curation, Conceptualization. **Stephan Gräf:** Writing – review & editing, Writing – original draft, Visualization, Validation, Supervision, Software, Project administration, Methodology, Investigation, Funding acquisition, Formal analysis, Data curation, Conceptualization.

Declaration of competing interest

The authors declare that they have no known competing financial interests or personal relationships that could have appeared to influence the work reported in this paper.

Acknowledgements

This work was funded by the Deutsche Forschungsgemeinschaft (DFG, German Research Foundation) – Project Number 530345255.

Data availability

Data will be made available on request.

